

Article

FOXP3 Isoforms Expression in Cervical Cancer: Evidence about the Cancer-Related Properties of FOXP3 Δ 2 Δ 7 in Keratinocytes

Natalia Garcia-Becerra ^{1,2}, Marco Ulises Aguila-Estrada ², Luis Arturo Palafox-Mariscal ^{1,2}, Georgina Hernandez-Flores ², Adriana Aguilar-Lemarroy ^{2,*}  and Luis Felipe Jave-Suarez ^{2,*} 

¹ Programa de Doctorado en Ciencias Biomédicas, Centro Universitario de Ciencias de la Salud, Universidad de Guadalajara, Guadalajara 44340, Mexico

² División de Inmunología, Centro de Investigación Biomédica de Occidente (CIBO), Instituto Mexicano del Seguro Social (IMSS), Guadalajara 44340, Mexico

* Correspondence: adry.aguilar.lemarroy@gmail.com (A.A.-L.); lfjave@gmail.com (L.F.J.-S.)

Simple Summary: FOXP3 is a critical transcription factor that works as a master regulator of the lymphoid lineage. The expression of FOXP3 was also observed in tumor cells; in cervical cancer, FOXP3 increases as the tumor progresses. However, the biological role of FOXP3 in cervical pathology is not well understood. In addition, FOXP3 has isoforms that could have different biological properties. In this work, the expression of FOXP3 and its isoforms were evaluated. It was found that the isoform FOXP3 Δ 2 Δ 7 is expressed in the cervical cancer-derived cell line SiHa. The transduction of this isoform in nontumorigenic keratinocytes induces proliferation, cell division, and migration. RNAseq analysis indicated that the FOXP3 Δ 2 Δ 7 isoform induces the expression of different protooncogenes and modulates essential pathways related to the immune response and the tumorigenic process.



Citation: Garcia-Becerra, N.; Aguila-Estrada, M.U.; Palafox-Mariscal, L.A.; Hernandez-Flores, G.; Aguilar-Lemarroy, A.; Jave-Suarez, L.F. FOXP3 Isoforms Expression in Cervical Cancer: Evidence about the Cancer-Related Properties of FOXP3 Δ 2 Δ 7 in Keratinocytes. *Cancers* **2023**, *15*, 347. <https://doi.org/10.3390/cancers15020347>

Academic Editor: Xavier Sastre-Garau

Received: 17 December 2022

Revised: 3 January 2023

Accepted: 3 January 2023

Published: 5 January 2023



Copyright: © 2023 by the authors. Licensee MDPI, Basel, Switzerland. This article is an open access article distributed under the terms and conditions of the Creative Commons Attribution (CC BY) license (<https://creativecommons.org/licenses/by/4.0/>).

Abstract: Cervical cancer (CC) is the fourth most common type of cancer among women; the main predisposing factor is persistent infection by high-risk human papillomavirus (hr-HPV), mainly the 16 or 18 genotypes. Both hr-HPVs are known to manipulate the cellular machinery and the immune system to favor cell transformation. FOXP3, a critical transcription factor involved in the biology of regulatory T cells, has been detected as highly expressed in the tumor cells of CC patients. However, its biological role in CC, particularly in the keratinocytes, remained unclarified. Therefore, this work aimed to uncover the effect of FOXP3 on the biology of the tumoral cells. First, public databases were analyzed to identify the *FOXP3* expression levels and the transcribed isoforms in CC and normal tissue samples. The study's findings demonstrated an increased expression of FOXP3 in HPV16+ CC samples. Additionally, the *FOXP3* Δ 2 variant was detected as the most frequent splicing isoform in tumoral cells, with a high differential expression level in metastatic samples. However, the analysis of *FOXP3* expression in different CC cell lines, HPV+ and HPV-, suggests no relationship between the presence of HPV and *FOXP3* expression. Since the variant *FOXP3* Δ 2 Δ 7 was found highly expressed in the HPV16+ SiHa cell line, a model with constitutive expression of *FOXP3* Δ 2 Δ 7 was established to evaluate its role in proliferation, migration, and cell division. Finally, RNAseq was performed to identify differentially expressed genes and enriched pathways modulated by *FOXP3* Δ 2 Δ 7. The exogenous expression of *FOXP3* Δ 2 Δ 7 promotes cell division, proliferation, and migration. The transcriptomic analyses highlight the upregulation of multiple genes with protumor activities. Moreover, immunological and oncogenic pathways were detected as highly enriched. These data support the hypothesis that *FOXP3* Δ 2 Δ 7 in epithelial cells induces cancer-related hallmarks and provides information about the molecular events triggered by this isoform, which could be important for developing CC.

Keywords: FOXP3; FOXP3 Δ 2 Δ 7; cervical cancer; HPV; RNAseq; GSEA

1. Introduction

Cervical cancer (CC) is one of the most preventable and treatable types of cancer due to the extended precancerous phase that lasts decades, yet it is still recognized as a health burden in low- and middle-income countries where it is ranked as the fourth most common type of cancer [1,2] and the second leading cause of cancer death, both in women and men [3]. The most frequent histopathologic subtype of CC is squamous cell carcinoma (SCC), which accounts for nearly 75–85% of the cases, and it is derived from the transformation of squamous cells at the external portion of the cervix, termed ectocervix, and the adenocarcinoma (ADC), with approximately 10–25% of CC cases, which is a consequence of columnar epithelial cells transformation at the endocervix, the internal portion of the organ [4–6]; there is also a third subtype named as adenosquamous carcinoma (ADSC), which accounts for merely 2–3% and is originated by a merge of both squamous and glandular cells [5].

The main risk factor for CC is persistent infection by high-risk human papillomavirus (hr-HPV), such as the 16 and 18 genotypes, which both are associated with approximately 70% of cases worldwide [7,8]; HPV16 is frequently associated with SCC, while HPV18 is associated with ADC [9]. Hr-HPVs stimulate cell transformation over decades through the constant expression of their oncoproteins to activate immunological and carcinogenic pathways to favor tumorigenesis and modulate local immunity [10–13].

FOXP3, forkhead box p3, is a member of the transcription factor family known as forkhead/winged helix; its locus is in the short arm of the X chromosome, which transcribes for an mRNA of 11 protein-coding exons. Interestingly, by alternative splicing, five isoforms could arise from the FOXP3 mRNA; these are *FOXP3-FL*, *FOXP3Δ2*, *FOXP3Δ7*, *FOXP3Δ2Δ3*, and *FOXP3Δ2Δ7* [14,15]. FOXP3 is recognized as a master regulator responsible for immune tolerance through the modulation of genetic and functional programs in regulatory T cells (Treg) [16]. The increase in Tregs in cancer is associated with a worse prognosis due to their immunosuppressive functions. The suppressive properties of Tregs rely on stable FOXP3 expression [16–18]. The two major isoforms of FOXP3 reported in Tregs are *FOXP3-FL* and *FOXP3Δ2*, which are expressed in approximately equal amounts; the main functional difference between both isoforms is derived from the inability of *FOXP3Δ2* to inhibit ROR α and ROR γ t functions [19–21]. A recently published study suggested that the expression of FOXP3 is closely related to the occurrence and growth of cervical cancer [22]. The expression of FOXP3 correlates with the prognosis of cervical cancer, and it is significantly higher in cancer than in cervical intraepithelial neoplasia or chronic cervicitis [22]. However, it remains unanswered whether there is a correlation between Tregs FOXP3+ and hr-HPV infection [23]. Nowadays, it is known that the FOXP3 expression is not exclusive of lymphoid lineage as it has been detected in epithelial cells from the breast, lung, prostate [24], and retinal tissue [25], as well as in cancer cells [26,27].

The role of FOXP3 in tumor cells is, however, controversial. It has been observed in breast and prostate cancer cells that FOXP3 expression is associated with antitumoral roles [28–31]. Furthermore, in ovarian cancer cells, inhibitory properties in proliferation, migration, and invasion were observed when FOXP3 was upregulated [32]. Conversely, the FOXP3 increase has also been linked to protumor functions in pancreatic, colorectal, gastric, bladder, thyroid, cervical, and nonsmall cell lung cancer [33–38]. In CC, the FOXP3 expression increased as the lesion progressed [39]. In addition, the knockdown of FOXP3 diminishes the growth of the SiHa cells [40]. However, whether the FOXP3 expression is regulated by HPV, which isoform is expressed in normal and tumoral keratinocytes, and the implications of FOXP3 expression in nontumorigenic epithelial cells are questions that remain unanswered. Therefore, this work aimed to evaluate the role of FOXP3 in the biology of keratinocytes and its contribution to the development of CC.

2. Materials and Methods

2.1. Cell Culture

SiHa, CaSki, HeLa, SW756, C33A, HaCaT, and Lenti-X 293T cell lines were cultivated in Dulbecco's Modified Eagle Medium (DMEM) with D-glucose (4.5 g/L) (No. Cat. 10-013-CV, Sigma-Aldrich, St. Louis, MI, USA), L-glutamine (584 mg/L), penicillin (100 U/mL), streptomycin (100 µg/mL), sodium pyruvate (110 mg/L), and 10% fetal bovine serum (FBS). Cells were maintained at 37 °C and a 5% CO₂ atmosphere in an incubator (C170UL-120V-R, Binder, Tuttlingen, Germany).

2.2. FOXP3Δ2Δ7 Open Reading Frame Cloning

The open reading frame (ORF) of FOXP3Δ2Δ7 was amplified through conventional PCR with DreamTaq Green PCR Master Mix (Cat. No. K1081, Thermo Scientific, Waltham, MA, USA) according to the manufacturers' instructions; cDNA from SiHa cells was used as a template. Primer sequences were designed using the Primer-BLAST tool from NCBI [41] (Table 1). The PCR product (1347 pb) was resolved by electrophoresis in 0.8% agarose gel, cut, and purified with Zymoclean Gel DNA Recovery Kit (Cat. No. D4001/D4002, ZYMO RESEARCH Corporation, Irvine, CA, USA) according to their instructions. The amplicon was ligated into the pGEM-T Easy vector (Cat. No. A137A, Promega, Madison, WI, USA) with T4 DNA Ligase (Cat. No. M180A, Promega, Madison, WI, USA) overnight at 4 °C. The ligation reaction was transformed into competent TOP10 bacteria by thermal shock and selected by the white/blue method. The constructed plasmid was named pGEM-FOXP3Δ2Δ7; from this, plasmid preparations were performed using the QIAprep Spin Miniprep Kit (Cat. No. 27106, QIAGEN Inc., Valencia, CA, USA).

Table 1. Primers sequences.

Gene	Forward	Reverse	Amplicon Size
FOXP3 ¹	5' ACA AGC CAG GCT GAT CCT T 3'	5' CAC ATC CAG GGC CTA TCA TC 3'	1347 bp
FOXP3 ²	5' CAA GTT CCA CAA CAT GCG ACC 3'	5' GCT CTC CAC CCG CAC AAA 3'	208 bp
SATB1 ²	5' CCT CAG CCA GAA CGT GAT GC 3'	5' GAC TCT GCT GGA GAG GCC A 3'	236 bp
CIR ²	5' AAG ATT CCT CGG TGC TTG CC 3'	5' GTT GCT TTG CGC TTC GTG TT 3'	216 bp
GLI2 ²	5' CAA CAA TGA CAG TGG CGT GG 3'	5' CTG CCA CTG AAG TTT TCC AGG 3'	297 bp
LAMP3 ²	5' ACA TGC GGT GGT GAT GTT CC 3'	5' AGG CAG AGA CCA ACC ACG AT 3'	219 bp
NSG1 ²	5' TTC CTC ACC TGC GTC GTC TT 3'	5' AAC TTG CCC ATC CCG CTA AG 3'	297 bp
HSPB8 ²	5' GGT GGC ATT GTT TCT AAG A 3'	5' TAC TGG CAT CTC AGG TAC AG 3'	208 bp
RPLP0 ²	5' CCT CAT ATC CGG GGG AAT GTG 3'	5' GCA GCA GCT GGC ACC TTA TTG 3'	95 pb
RPL32 ²	5' GCA TTG ACA ACA GGG TTC GTA G 3'	5' ATT TAA ACA GAA AAC GTG CAC A 3'	320 pb

¹ Primer used for gene cloning. ² Primer used for quantitative PCR.

Subsequently, the FOXP3Δ2Δ7 ORF was isolated from the pGEM-FOXP3Δ2Δ7 vector by restriction with EcoRI (No. Cat. IVGN0116, Invitrogen, Waltham, MA, USA) and sub-cloned into the lentiviral vector pLVX-Puro (Cat. No. 632164, Clontech Laboratories Inc., Mountain View, CA, USA) that was previously linearized with EcoRI, and dephosphorylated with Antarctic Alkaline Phosphatase (Cat. No. IVGN2204, Invitrogen, Waltham, MA, USA). The resulting plasmid pLVX-FOXP3Δ2Δ7 was used to sequence the FOXP3Δ2Δ7 ORF using the Big Dye v3.1 Terminator Cycle Sequencing kit (Cat. No. 4337455, Applied Biosystems, Thermo Fisher Scientific Inc., Waltham, MA, USA), and the ABI PRISM 310 Genetic Analyzer (Applied Biosystems). The sequences were aligned using the UGENE software (v.1.21.1) [42]. The NCBI sequences NM_014009.3 and NM_001114377.1 were used as references.

Finally, the plasmid pLVX-FOXP3Δ2Δ7 was used to obtain lentiviral particles.

2.3. Production of Lentiviral Particles

Lenti-X 293T cell line (Cat. No. 632180, Clontech Laboratories Inc., Mountain View, CA, USA) was used as viral producer cells; 4 × 10⁶ cells were seeded in p100 plates and cultured for 24 h. Plasmids-lipofectamine 2000 complexes were prepared as follows,

both lipofectamine 2000 reagent (Cat. No. 11668019, Invitrogen, Waltham, MA, USA) and plasmids pLVX-FOXP3 Δ 2 Δ 7, pCMVR8.74 (Addgene 22036), and pMD2.G (Addgene 12259) were separately diluted in DMEM-free FBS medium. The plasmids pCMVR8.74 and pMD2.G were used to produce the necessary packaging proteins for lentiviral production.

After 5 min of incubation at room temperature, both solutions, diluted plasmids and diluted Lipofectamine 2000 reagent, were gently mixed and incubated for 20 min at room temperature. Finally, the plasmid-lipofectamine complexes were added to the cells, and the plate was mixed by gently rocking back and forth.

After 48 h, the supernatants of transfected cells were collected and filtered through a 0.45- μ m PES filter to eliminate detached cells, aliquoted, and subsequently stored at -80°C until use. Viral titer was determined by qPCR from 100 μ L of supernatant.

2.4. HaCaT Cell Transduction

HaCaT cells were infected with at least 5 IFU per cell of lentiviral particles containing the FOXP3 Δ 2 Δ 7 ORF. After 72 h of infection, 0.5 μ g/mL of puromycin (Cat. No. A1113803, Gibco, Waltham, MA, USA) was added to the cell culture. The cells were left under these conditions for another 72 h. After that, the cells were cultured in media with 0.1 μ g/mL of puromycin for two more weeks or until no surviving cells were observed in the noninfected control plate. Following this procedure, two cell lines were obtained: HaCaT-LVX (transduced with the empty vector as control) and HaCaT-FOXP3 Δ 2 Δ 7.

2.5. Quantitative PCR

Total RNA was extracted with the Quick-RNA miniprep plus kit (Cat. No. R1058, Zymo Research, Irvine, CA, USA) according to the manufacturers' instructions. SuperScript II reverse transcriptase (Cat. No. 18064022, Invitrogen, Waltham, MA, USA) and 5 μ g of total RNA were used for the cDNA synthesis.

The quantitative PCR (qPCR) was performed on the LightCycler 2.0 equipment (Roche Diagnostics, Basel, Switzerland) with the LightCycler FastStart DNA Master plus SYBR Green I Kit (Cat. No. 03515869001, Roche Diagnostics, Basel, Switzerland). *RPLP0* and *RPL32* were used as reference genes. The sequences of all primers used (*FOXP3*, *SATB1*, *C1R*, *GLI2*, *LAMP3*, *NSG1*, *HSPB8*, *RPLP0*, and *RPL32*) can be found in Table 1.

2.6. Proliferation Assay (xCELLigence)

Cells (5000) were seeded in triplicate in an xCELLigence Real-Time Cell Analysis (RTCA) 96-well electronic microplate (E-Plate 96) (Cat. No. 300601010, Agilent Technologies, Inc., Santa Clara, CA, USA) and incubated for 48 h with impedance detection every hour with the xCELLigence RTCA SP station (Agilent Technologies, Inc., Santa Clara, CA, USA). Proliferation was measured as cell index change over time.

2.7. Cell Division Tracking

CSFE Cell Division Tracker Kit (Cat. No. 423801, BioLegend, San Diego, CA, USA) was used for cell division analysis. CSFE (carboxyfluorescein succinimidyl ester) reactant was diluted with DMSO (Cat. No. D8418-250ML, Sigma-Aldrich, St. Louis, MO, USA) to prepare a 5 mM solution. In a 60 mm plate, 50,000 cells were seeded and incubated until the next day. A 5 mM working solution was prepared in DMEM media without FBS. The cells were incubated with the working solution for an hour, then the media was changed, and fresh DMEM with 10% FBS was added. The cells were kept growing for 72 h until the fluorescence measurement by flow cytometry was performed. The cells were measured right before the incubation for the initial time detection.

2.8. Cell Migration Assay

For the cell migration assay, 800,000 cells were seeded in a 6-well plate (Cat. No. 140675, Thermo Fisher Scientific Inc., Waltham, MA, USA) for 24 h until full confluence was reached. A new media with 10 μ g/mL mitomycin C (Cat. No. 10107409001, Roche

Diagnostics, Basel, Switzerland) was added to avoid proliferation bias. After two hours of incubation with mitomycin C, three straight lines and one horizontal line, as a reference, were manually created with a 200- μ L sterile pipette tip on each cell group and its duplicate; the plate was washed twice with PBS to remove nonadherent cells, and finally, fresh media was added.

Photographs were acquired at 0, 12, and 24 h with the 4x objective of a ZEISS inverted microscope (Primo Vert No. 415510-1101-000 model, Carl Zeiss Microscopy GmbH, Jena, Germany), with a ZEISS AxioCam camera (Erc5s model, Carl Zeiss Microscopy GmbH, Jena, Germany), and the ZEN 2012 software (Blue edition, Carl Zeiss Microscopy GmbH, Jena, Germany). Data obtained were analyzed to evaluate the percentage of wound closure with ImageJ software (Image Processing and Analysis in Java; Rasband, W.S., ImageJ, U.S. National Institutes of Health, Bethesda, MD, USA, <https://imagej.nih.gov/ij/>, accessed on 23 April 2022).

2.9. RNAseq

Next-generation RNA sequencing with the Nova Seq 6000 Illumina platform was conducted by Novogen Bioinformatics Technology Co., Ltd. (Beijing, China); independent sample duplicates of total RNA from HaCaT-LVX and HaCaT-FOXP3 Δ 2 Δ 7 were sent and preserved in RNastable (Cat. No. 93221-001, Biomatrix, San Diego, CA, USA).

Retrieved data was analyzed in both open-source platforms, Rstudio (version 1.4.1717) [43], and Galaxy (version 22.05.1) (<https://www.usegalaxy.org> accessed on 3 February 2022) [44].

The sequencing quality of the returned data (FASTQ archives) was analyzed with FASTQC (version 0.11.9) [45]. Subsequently, alignment to the Homo sapiens genome (version 42) (GRCh38.p13) was performed with the Subjunc aligner (version 2.0.0) [46] from the Rsubread package (version 3.14) [46]. Afterward, BAM files were processed with featureCounts (version 2.0.1) [47]. Normalization of read counts as FPKM (fragments per kilobase of exon per million mapped fragments) was achieved using the DESeq2 tool (version 1.36.0) [48].

Selection of the differentially expressed genes (DEGs) was defined by $-1.5 \leq \text{Log}_2(\text{fold change}) \leq 1.5$ and $p\text{-value} < 0.05$ as selection criteria.

2.10. Gene Set Enrichment Analysis

From the data obtained by the DESeq2 tool, two matrices were generated, the first in a tab-delimited text file with the normalized expression data in FPKM and the second in a cls file with the identification of the phenotypes. Both matrices were loaded in GSEA software (version 4.2.2) [49], the “Hallmark” gene set database (h.all.v2022.1.Hs.symbols.gmt) was selected, and for the *Chip Platform*, the “Human_Gene_Symbol_with_Remapping_MsigDB.v7.5.1.chip” option was chosen. One thousand phenotype permutations were established, and the Signal2Noise parameter was selected in the *metric for ranking genes* configuration. Finally, an FDR value < 0.25 was chosen to identify significant enriched pathways.

2.11. Statistics

All experiments were performed with at least two independent replicates; the two-way analysis of variance (ANOVA) and unpaired Student *t* tests were used to calculate differences between groups. A $p\text{-value} < 0.05$ was considered statistically significant.

3. Results

3.1. Augmented FOXP3 Expression in Cervical Cancer

To identify the expression profile of FOXP3 in CC samples, an expression analysis in OncoDB (<https://oncodb.org/> accessed on 7 September 2022) [50] was performed. Results from CC samples ($n = 304$) compared against normal tissue ($n = 22$) showed a significant increase in FOXP3 mRNA expression in tumor samples (Figure 1a). To identify if FOXP3 expression was related to the three most common CC subtypes, data collected from “Cervical Squamous Cell Carcinoma and Endocervical Adenocarcinoma (TCGA,

Firehoses Legacy)" ($n = 310$) in cBioPortal was assessed (<https://www.cbioportal.org/> accessed on 7 September 2022) [51,52]. The findings depict the *FOXP3* mRNA expression level by CC subtype as well as the frequency of positive samples for *FOXP3*; deriving from those values, *FOXP3* was detected in 98.8% of samples with SCC, 100% of ADC samples, and 80% of ADSC; moreover, *FOXP3* expression average in SCC was higher compared with the other two subtypes (Figure 1b).

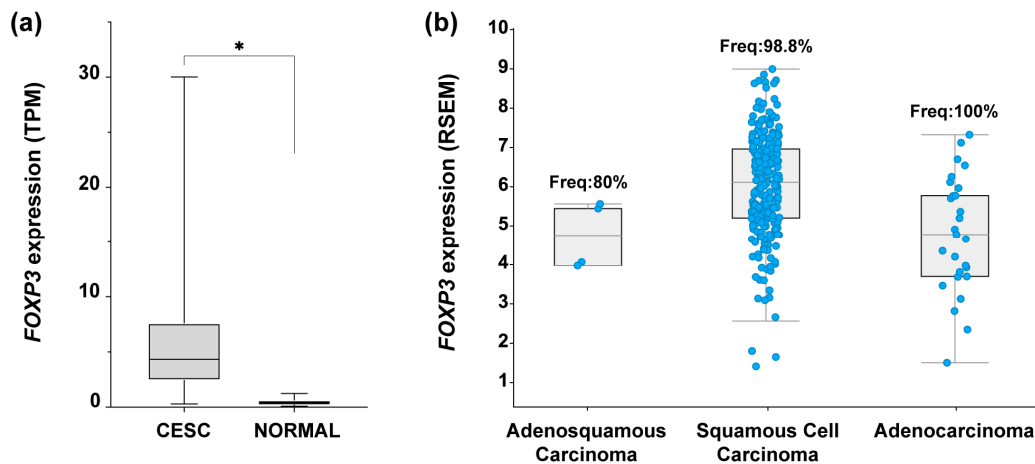


Figure 1. *FOXP3* expression levels in cervical cancer. (a) Comparison of *FOXP3* expression levels in transcript per million (TPM) from cervical epithelial squamous carcinoma (CESC) samples ($n = 304$, avg = 5.7, median = 4.3) vs. normal tissue (NORMAL) ($n = 22$, avg = 0.4, median = 1), $\text{Log}_2(\text{Fold Change}) = 2.1$; (b) *FOXP3* expression abundance in RNA Seq by expectation-maximization (RSEM) from TCGA-CESC data; RSEM values are expressed as RNA Seq V2 RSEM ($\text{Log}_2(\text{value} + 1)$). Each blue dot represents a patient sample positive for *FOXP3* expression: adenosquamous carcinoma, $n = 4$ of 5 (frequency = 80%), squamous cell carcinoma, $n = 253$ of 256 (frequency = 98.8%), adenocarcinoma, $n = 27$ of 27 (frequency = 100%); TCGA-CESC, $n = 308$ patients. (*) depicts statistical significance with a p -value < 0.05 .

3.2. *FOXP3* $\Delta 2$ Is the Most Prevalent Variant in Cervical Cancer Samples, and Its Expression Is Highly Differential in Metastatic Stages

To deepen into the *FOXP3* mRNAs isoforms expressed in cervical cancer, data from TCGA-CESC was analyzed in ISOexpresso (<http://wiki.tgilab.org/ISOexpresso/> accessed on 10 October 2022) [53] and TSVdb (<http://tsvdb.com/> accessed on 10 October 2022) [54] web-based platforms. Results obtained from the analyses showed that tumor samples express three variants with a differential frequency, *FOXP3* $\Delta 2$ with a frequency of 74%, *FOXP3* $\Delta 7$ with 17%, and *FOXP3* X1 with 9% (Figure 2a). TSVdb results showed that the most frequent variant, *FOXP3* $\Delta 2$, was expressed with a high difference between normal and metastatic tissue (Figure 2b). The *FOXP3* $\Delta 7$ variant was observed with slightly increased expression in primary solid tumors, but no difference was observed for normal and metastatic samples (Figure 2c). Unfortunately, the *FOXP3* $\Delta 2\Delta 7$ variant is not included in these databases. Therefore, no information related to this isoform was available in either database.

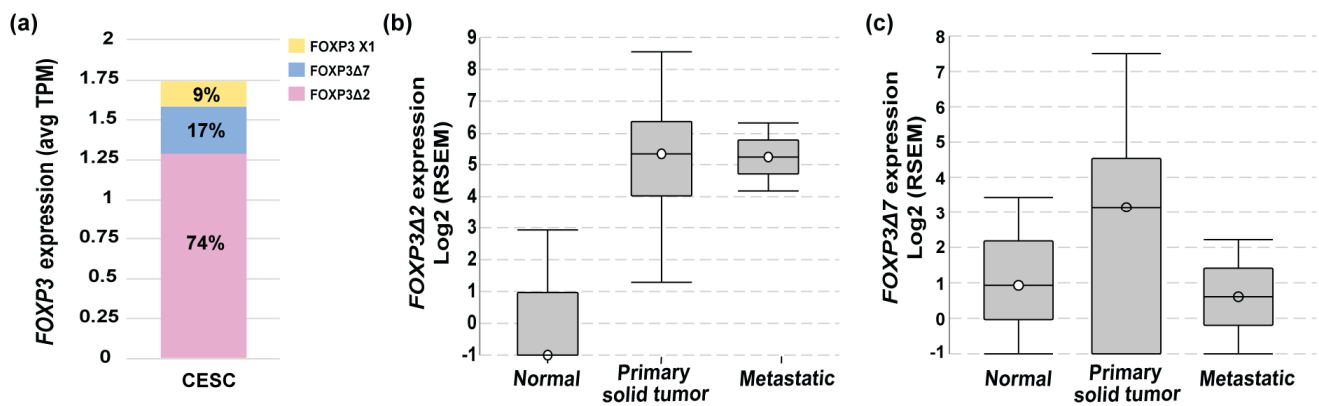


Figure 2. *FOXP3* variant levels in cervical cancer. (a) *FOXP3* expression levels and variant frequencies in transcripts per million (TPM) from TCGA-CESC data ($n = 305$); (b) *FOXP3Δ2* expression abundance in RNA Seq by expectation-maximization (RSEM) in normal ($n = 1$ of 3), primary solid tumor ($n = 273$ of 304) and metastatic ($n = 2$ of 2); TCGA-CESC, $n = 309$; (c) *FOXP3Δ7* expression abundance in RNA Seq by expectation-maximization (RSEM) in normal ($n = 2$ of 3), primary ($n = 222$ of 304), and metastatic solid tumors ($n = 1$ of 2); TCGA-CESC $n = 309$.

3.3. HPV16 Infection Could Increase *FOXP3* Expression Levels in Cervical Cancer

The main etiological factor for developing CC is persistent infection with high-risk HPV, such as 16 or 18 genotypes. To identify if there is an association between the HPV presence and the *FOXP3* increase, *FOXP3* expression levels in CC samples HPV16+ and HPV18+ from OncoDB were analyzed. Results obtained from OncoDB showed an increase in *FOXP3* expression in the presence of both genotypes but with a marked difference in HPV16+ samples, in which a greater tendency of overexpression was observed compared to the HPV18+ and HPV(-) CC samples (Figure 3a).

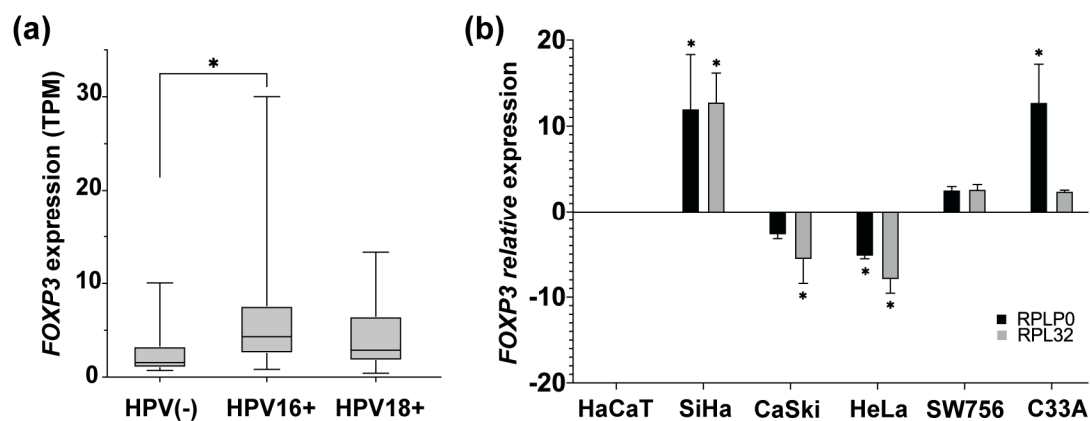


Figure 3. *FOXP3* expression levels in cervical cancer samples and cervical cancer-derived cell lines. (a) Comparison of *FOXP3* expression levels in transcript per million (TPM), from CC samples HPV16+ and HPV18+ vs. HPV(-) CC samples; (b) detection of *FOXP3* relative expression levels by qPCR in CC-derived cell lines HPV16+ (SiHa and CaSki), HPV18+ (HeLa and SW756), and HPV(-) (C33A); *RPLP0* and *RPL32* were used as reference genes. The expression of *FOXP3* in HaCaT cells was used as a calibrator. (*) depicts statistical significance with a p -value < 0.05 .

After that, it was of interest to determine the status of *FOXP3* expression in CC-derived cell lines HPV16+ (SiHa and Ca Ski), HPV18+ (HeLa and SW756), HPV(-) (C33A), and nontumorigenic keratinocytes (HaCaT). The relative expression level of *FOXP3* was assessed by qPCR and compared to the expression of HaCaT cells. The results indicated high relative expression in SiHa cells. However, CaSki cells, equally positive for HPV16, showed decreased expression of *FOXP3*. On the other hand, HPV18-positive cell lines

express differentially *FOXP3* levels, HeLa cells with a subexpression and a slight increase in the SW756 line. Regarding the C33A cell line (HPV negative), a trend of overexpression was observed (Figure 3b).

The evidence so far supports that *FOXP3* expression tends to increase in cervical cancer and HPV-positive cervical samples. However, in the panel of CC-derived cell lines analyzed, only the SiHa and C33A cell lines seem to maintain this feature. To have some insights into the molecular implications of *FOXP3* expression, we selected the SiHa cell line. Therefore, the *FOXP3* ORF from this cell line was isolated, cloned, and sequenced. The findings showed that SiHa cells express the *FOXP3Δ2Δ7* variant (Figure 4b), an isoform of *FOXP3* are poorly studied; then, the derived question was to know whether the *FOXP3Δ2Δ7* varies the shapes and behavior of nontumorigenic keratinocytes.

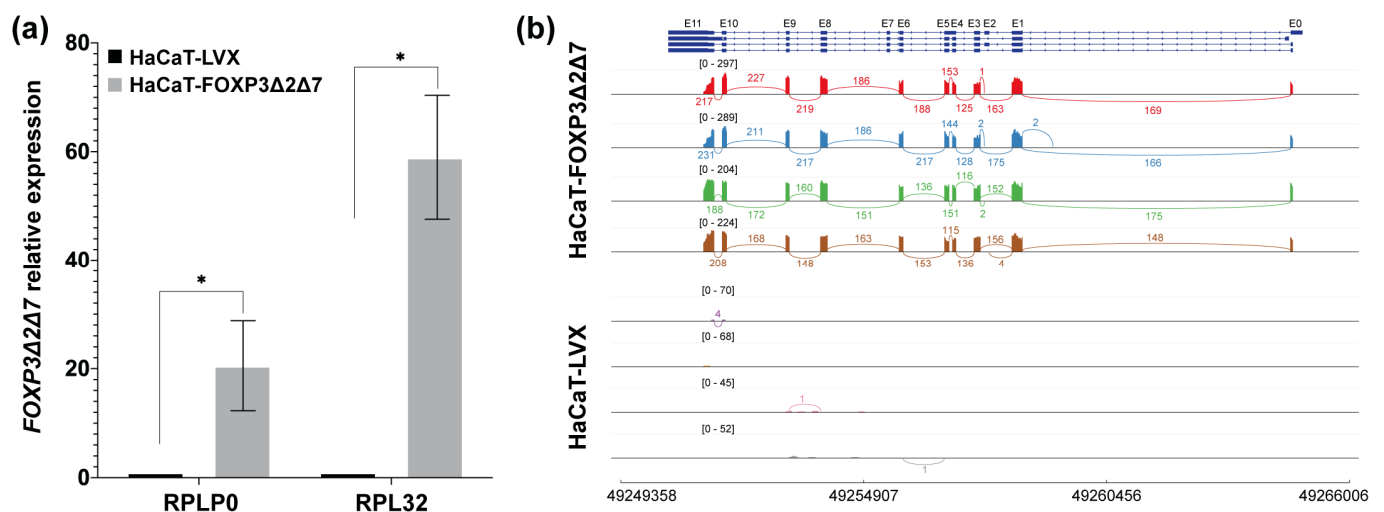


Figure 4. Validation of the establishment of the *FOXP3Δ2Δ7* exogenous expression model. (a) *FOXP3Δ2Δ7* relative expression levels were detected in the cell model by qPCR; *RPLP0* and *RPL32* were used as reference genes. The expression of *FOXP3* in HaCaT-LVX was used as a calibrator to calculate the relative expression; (b) Sashimi plot of the RNAseq assays from replicates of HaCaT-*FOXP3Δ2Δ7* and HaCaT-LVX cell lines, reads covering the *FOXP3* genomic region are shown as colored peaks, and each numbered curved line represents an interexonic junction with the detection level. Upper blue boxes and connecting blue lines represent exonic and intronic regions. (*) depicts statistical significance with a *p*-value < 0.05.

3.4. Exogenous Expression of *FOXP3Δ2Δ7* Promotes Cell Proliferation, Division, and Migration

Once the *FOXP3Δ2Δ7* ORF from SiHa was subcloned and stably transduced into HaCaT cells, validation of the lentiviral transduction was assessed by qPCR and RNAseq. The results demonstrated a significant increase in *FOXP3*'s relative expression in HaCaT-*FOXP3Δ2Δ7* (Figure 4a). Furthermore, the RNAseq analysis of the transduced model shows abundant reads covering the genomic region corresponding to the *FOXP3* gene. It was also possible to observe the lack of exons 2 and 7, confirming that the mRNA isoform expressed by HaCaT-transduced cells was the *FOXP3Δ2Δ7* version (Figure 4b).

To identify the effect of *FOXP3Δ2Δ7* exogenous expression in cell proliferation, cell index determination by impedance with the xCELLigence RTCA platform was performed (Figure 5a); results exhibit an increase in cell index when compared with control. Additionally, cell division tracking assays revealed a diminished fluorescence in *FOXP3Δ2Δ7*-expressing cells, which indicates a higher cell division rate (Figure 5b). Further, wound healing assays showed that *FOXP3Δ2Δ7* significantly promoted the migration process (Figure 5c).

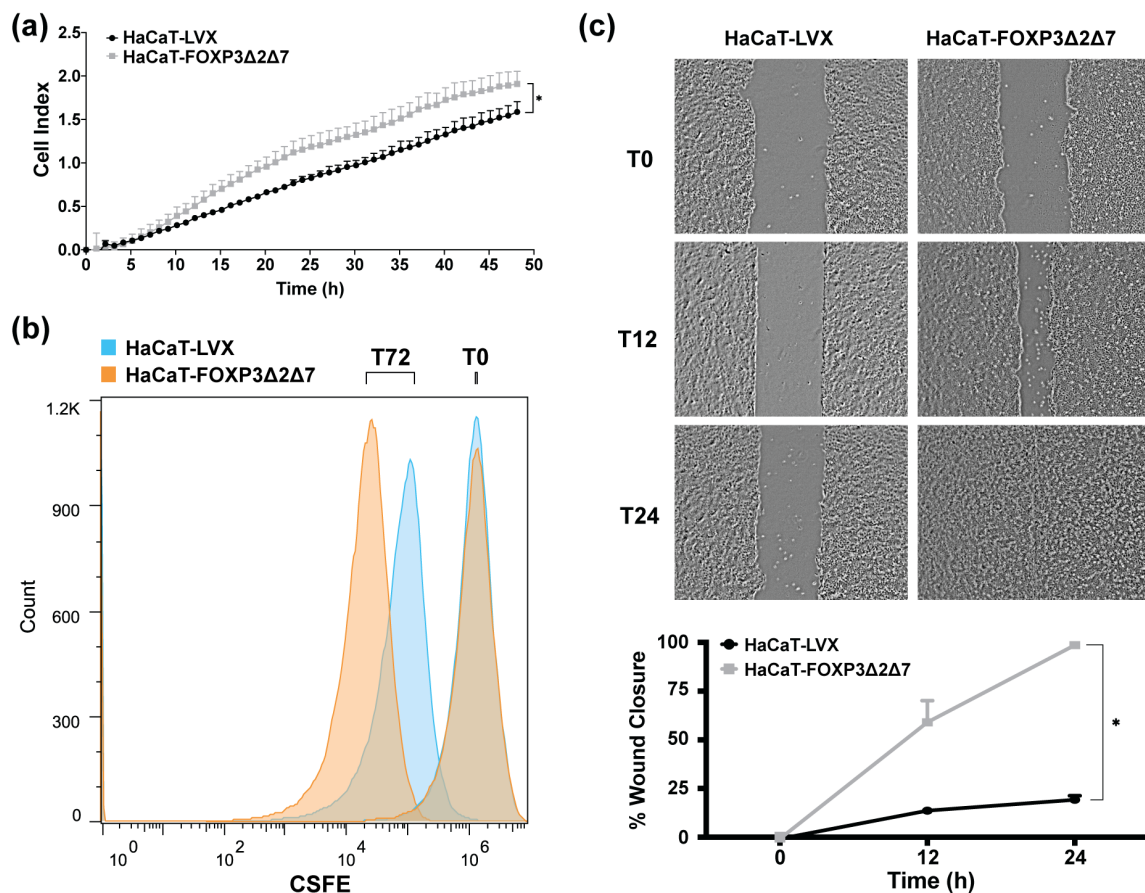


Figure 5. Evaluation of biological effects by *FOXP3Δ2Δ7* exogenous expression in vitro. (a) Real-time cell proliferation analysis with xCELLigence RTCA platform for 48 h; values are expressed as cell index; (b) cell division tracking with CSFE reagent, fluorescence measurement was achieved with flow cytometry at the initial time point and 72 h later; (c) depictive images of wound healing assay and plot of wound closure percentage during 24 h; photographs were acquired at 4× amplification and processed with ImageJ software. (*) depicts statistical significance with a p -value < 0.05.

3.5. Exogenous Expression of *FOXP3Δ2Δ7* Induces the Transcription of Protumoral Genes and the Enrichment of Immunological and Oncogenic Pathways

Next-generation sequencing of total mRNA was performed to comprehend the molecular mechanisms behind the protumorigenic activities induced by the exogenous expression of *FOXP3Δ2Δ7*. RNAseq assays highlighted differentially expressed genes. Using the selection criteria of $-1.5 \leq \text{Log}_2(\text{fold change}) \leq 1.5$ and a p -value < 0.05, the results showed 23 upmodulated genes and 27 downmodulated genes. As expected, *FOXP3* was the most overexpressed gene with a $\text{Log}_2(\text{fold change})$ of 6.84, and among the 23 upregulated genes, numerous are associated with protumorigenic functions (Figure 6a). To validate the RNAseq results, the genes *SATB1*, *C1R*, *GLI2*, *LAMP3*, *NSG1*, and *HSPB8* were selected and analyzed by qPCR (Figure 6b,c); the results show a global trend towards the upregulation of pro-oncogenic genes.

Furthermore, for the recognition of *FOXP3Δ2Δ7* modulated pathways, enrichment analysis was performed by using the GSEA software. For a confident selection of modulated pathways, an FDR q -value < 0.25 was used. Among the pathways modulated by *FOXP3Δ2Δ7*, several are involved in the immune response (e.g., complement, inflammatory response, IL2/STAT5 signaling, IL6/JAK-STAT signaling), and others have been associated with oncogenic processes (e.g., KRAS, WNT/beta-catenin, hypoxia) (Figure 7).

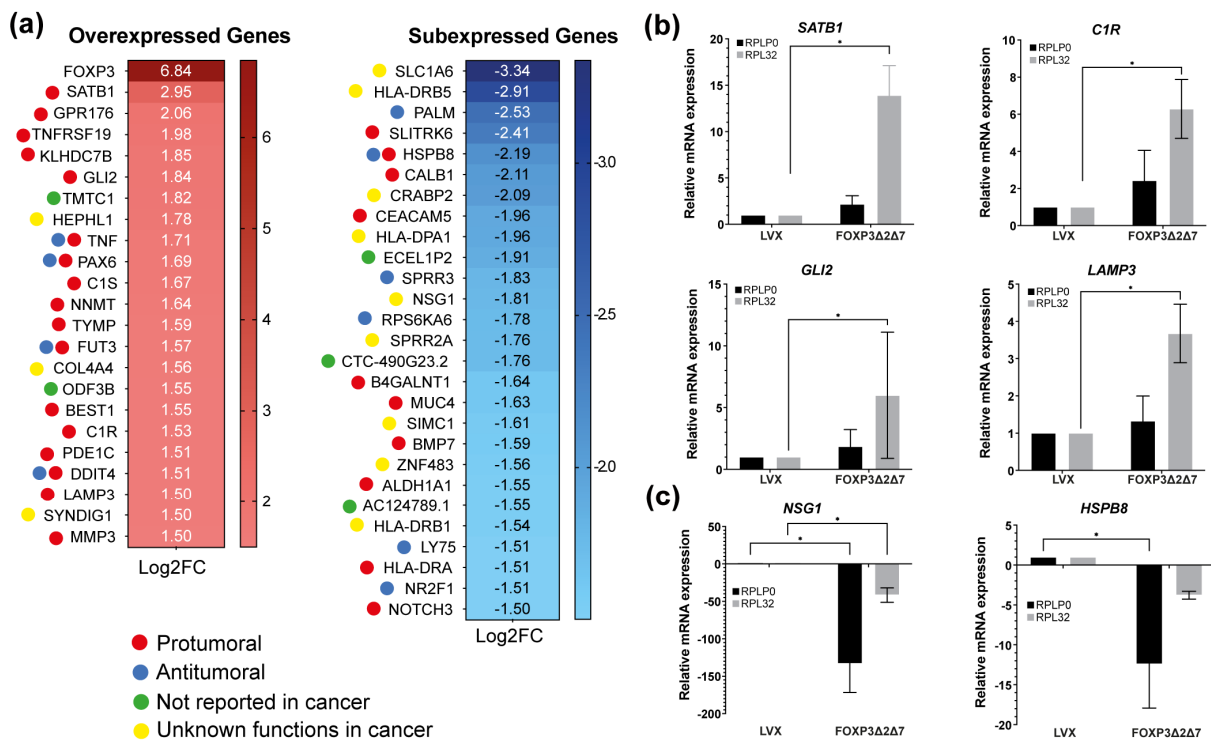


Figure 6. Identification of differentially expressed genes by *FOXP3Δ2Δ7* exogenous expression. (a) Differentially expressed genes heatmap selected by $-1.5 \leq \text{Log}_2(\text{fold change}) \leq 1.5$, p -value < 0.05 ; code color indicates a review of what has been previously published about that gene; (b) relative mRNA expression of upregulated genes by qPCR; *RPLP0* and *RPL32* were used as reference genes; (c) relative mRNA expression of downregulated genes by qPCR; *RPLP0* and *RPL32* were used as reference genes. (*) depicts statistical significance with a p -value < 0.05 .

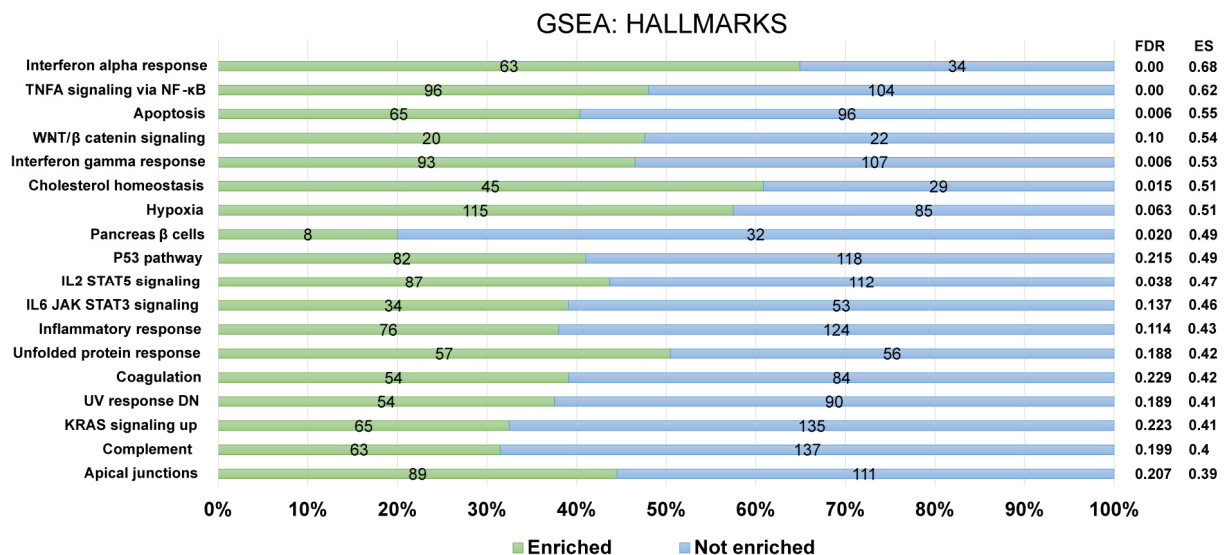


Figure 7. Identification of enriched biological pathways modulated by *FOXP3Δ2Δ7* exogenous expression. Enrichment analysis from the Hallmark gene set collection was assessed by GSEA software. The left panel depicts the standard names of the statistically significant pathways, and the right panel shows the false discovery rate (FDR) and enrichment score (ES) values. The numerals at the bar plot indicate the number of enriched (green) and not enriched (blue) genes within each pathway. $FDR < 0.25$ was established as a selection criterion. A percentage scale is shown at the bottom for better visualization.

4. Discussion

FOXP3, a member of the transcriptional factor family forkhead/winged-helix, is commonly known as a master regulator of regulatory T CD4+ CD25+ cells, which promotes homeostasis and immunological tolerance. These functions are established through the transcriptional activation or repression of approximately 700 genes and miRNAs related to the TCR pathway, cell communication, and transcriptional regulation [55].

Nowadays, it is known that FOXP3 expression occurs not only in hematopoietic cells but also in cancer cells. Karanikas et al. reported high expression levels of FOXP3 in 25 cancer-derived cell lines [26]. Several studies have reported the FOXP3 expression increase in tumor cells, and in some cases with tumor suppressor activity, as in ovarian, prostate, and breast cancer [29,32,56], but also as an oncoprotein, as in gastric, bladder, lung, and cervical cancer, among others [37,38,40,57].

Since 2012, when the first report about FOXP3's increase in CC was published [39], its biological role in the development of cervical pathology has been unclear. Initial findings showed that FOXP3 overexpression was especially marked in CC samples [22,39,40]; in this work, such increased expression was also evident in HPV+ CC samples, particularly within the most frequent genotype, HPV16. These findings suggest that the increase in FOXP3 does not occur solely due to the presence of HPV but could also be dependent on the infecting genotype; Zeng et al., in 2012, established the hypothesis that the virus uses FOXP3 increase as an essential mechanism to control the immune system and to preserve the active infection [39]. To confirm or deny this last postulate, it is necessary to carry out more elaborated approaches.

On the other hand, the analysis of FOXP3 variants' frequencies highlights the FOXP3 Δ 2 isoform as the most common in CC samples. To the best of our knowledge, this is the first work analyzing FOXP3 variants in cervical cancer, particularly the FOXP3 Δ 2 Δ 7 variant, which was identified in the SiHa cell line. The relevant feature of losing the coding exon two region, or Δ 2, is the absence of a repression domain, which is believed to have tumor suppressor functions due to a possible transcriptional restriction of oncogenes [58]. Therefore, isoforms lacking could allow free transcription of normally repressed genes. On the other hand, the full-length variant, in which the coding exon two is present, should have opposite activities, and this is confirmed by the observations using breast and ovarian cancer cells, in which the introduction of the FOXP3-FL variant decreases tumor growth, inhibits proliferation, and decreases migration and invasion [29,32]. Additionally, the coding exon two loss was associated with greater aggressiveness and chemo-resistance in bladder cancer [57]. Moreover, in nonsmall cell lung cancer, it was related to increased proliferation, migration, and invasion [38]. The loss of the coding exon 7 (Δ 7) was previously documented in an isoform of FOXP3 [15], FOXP3 Δ 7 lacks an 81-bp region that contains part of the leucine zipper domain of the protein, which is necessary for protein-protein interactions, and it was postulated that mutations in the exon 7 prevent protein dimerization and, therefore, DNA binding [59]. Mutations in exon 7 were associated with an autoimmune disease called IPEX [60,61]. Nevertheless, Mailer et al., working with the FOXP3 Δ 2 Δ 7, found that the lack of exon 7 does not affect protein dimerization or interaction with RUNX1, NFAT, or NF- κ B [62]. However, the exogenous expression of FOXP3 Δ 2 Δ 7 failed to induce the typical Treg-associated phenotype in lymphocytes [62]. The latter indicates that FOXP3 Δ 2 Δ 7 has a different function compared with FOXP3-FL. In this work, we report the expression of FOXP3 Δ 2 Δ 7 in SiHa cells. The lentiviral transduction of FOXP3 Δ 2 Δ 7 in nontumorigenic keratinocytes stimulates cell proliferation and division. These results agree with the observations of Luo et al. [40]. They induced the silencing of FOXP3 by employing RNA interference in SiHa cells and observed a decrease in proliferation, migration, and invasion [40]. Evidence of an FOXP3 oncogenic behavior was also observed in gastric cancer [37]. Similarly to our work, the exogenous expression of FOXP3 induces both proliferation and migration, however, the authors do not provide information about the FOXP3 isoform [37]. All this evidence indicates the importance of determining not only the expression of FOXP3 but also the isoform that the cell is expressing.

Functional analyzes establish clear evidence of the protumoral capacity of *FOXP3Δ2Δ7* in vitro, to delve into the molecular mechanisms underlying the biological activities of this isoform transcriptomic analysis were performed. Among the overexpressed genes, *SATB1* highly increased. This gene is involved in the epithelial-mesenchymal transition [63–66], and its overexpression has been associated with a worse prognosis in solid tumors [67]. In CC, it was identified as highly expressed in those women who presented advanced stages of the disease and through a Kaplan–Meier analysis, it was possible to associate it as a worse prognosis marker [68].

Other gene upregulated was *GLI2*, it has been identified as a potent oncogene that mediates the hedgehog signaling pathway [69–71]; in CC it was shown that its subexpression inhibited the growth and migration of cell lines derived from cancer, and it was also associated as a poor prognostic marker based on TCGA data [72].

Regarding *C1R*, there is no information related to CC; however, what has been published to date relates this gene to tumor growth, vascularization, and invasion in cutaneous squamous cell carcinoma [73,74]. High levels of *C1R* were reported in nonsmall cell lung cancer compared to control groups. Interestingly, the high levels of this gene were associated with an increased risk of death [75].

LAMP3 was associated with increased migration in an overexpression model derived from a cervical cancer cell line, and an in vivo metastasis assay demonstrated that 9 of 11 *LAMP3* overexpressing mouse models elicited a process of distal metastasis with invasion of the lymphovascular space. Additionally, they demonstrated that in 100% of the CC samples, the gene was found to be overexpressed [76].

The enrichment analysis highlights important pathways modulated by *FOXP3Δ2Δ7* expression, some of them closely related to the immune response. It has been reported that *FOXP3* inhibits the activity of *NFAT* and *NF-κB*, two important transcription factors essential for cytokine expression [77]. These results agree with those reported in melanoma, which indicates that *FOXP3* in cancer cells modulates the expression of molecules associated with immunity, in addition to contributing to the recruitment of Treg lymphocytes, which establishes a suppressive activity that favors tumor progression [78].

On the other hand, several of the signaling pathways identified as enriched are recognized for their oncogenic potential. The *KRAS* signaling pathway is highly involved in cell proliferation and division; it belongs to the *RAS/MAPK* pathway, and in the oncogenic context, *KRAS* has very important effects in the carcinogenesis process of endometrial, colorectal, bladder, breast, and cervical cancer [79–86].

Regarding the *WNT/β-catenin* signaling pathway, it is involved in both the proliferation process and migration; in CC, it is recognized as a practically necessary pathway for cell transformation, which leads to an increase in the aforementioned processes [87], additionally, it is interesting to mention that the *SATB1* gene is related to the process of migration, and with the *WNT/β-catenin* pathway, this has been reported in colorectal cancer by promoting tumorigenesis, progression, and epithelial-mesenchymal transition [63,88].

Ultimately, it is important to mention that *FOXP3Δ2Δ7* modulates the hypoxia signaling pathway, this pathway involves genes activated in response to low oxygen concentrations. In cancer, this phenomenon is highly relevant for the establishment of cancer hallmarks and the activation of cellular processes that include proliferation, survival, tumor invasion, and metastasis [89–91]. In CC, as expected, high degrees of hypoxia are associated with a poor prognosis [92] and, interestingly, also with resistance to chemotherapeutics [93,94]. As well, it is pertinent to acknowledge the role of *LAMP3* in the pathway, as Mujcic et al. demonstrated in a cohort of human cervix tumors an increased expression of the gene as a consequence of hypoxia but furthermore, they found that *LAMP3* is an essential regulator of hypoxia-driven nodal metastasis [95].

Future research should aim to evaluate the role of *FOXP3Δ2Δ7* on the immune response regulation in the immune cells and tumor cells at the tumoral niche in CC.

5. Conclusions

The behavior of the FOXP3 expression during cervical cancer development was observed to increase. FOXP3 expression was also increased in HPV-positive samples, especially in those positive for HPV16. An analysis of the isoforms expressed in this pathology indicates the importance of the loss of the exon coding two of FOXP3. Functional studies suggest that isoform *FOXP3Δ2Δ7* presents a protumorigenic behavior when introduced into keratinocytes since it induces cell proliferation, migration, and division. Additionally, the transcriptomic analysis highlights the importance of this isoform in the modulation of pathways, such as interferon, apoptosis, TNF, hypoxia, IL-2, IL-6, and the inflammatory response, among others. The latter reveals the critical role the FOXP3 isoforms could play in modulating the immune response. Subsequent studies evaluating FOXP3 isoforms and their effect on immune cells will provide a better understanding of the immunomodulatory effects of FOXP3 expression in tumor cells.

Author Contributions: Conceptualization, N.G.-B., A.A.-L. and L.F.J.-S.; methodology, N.G.-B., M.U.A.-E. and L.A.P.-M.; software, N.G.-B. and L.F.J.-S.; validation, N.G.-B.; formal analysis, N.G.-B.; investigation, N.G.-B., M.U.A.-E., G.H.-F. and L.A.P.-M.; resources A.A.-L. and L.F.J.-S.; data curation, L.F.J.-S.; writing—original draft preparation, N.G.-B.; writing—review and editing, N.G.-B., A.A.-L. and L.F.J.-S.; visualization, N.G.-B., A.A.-L. and L.F.J.-S.; supervision, G.H.-F., A.A.-L. and L.F.J.-S.; project administration, A.A.-L. and L.F.J.-S.; funding acquisition, A.A.-L. and L.F.J.-S. All authors have read and agreed to the published version of the manuscript.

Funding: N.G.-B. is grateful to Consejo Nacional de Ciencia y Tecnología (CONACyT)-México for a financial support with a grant (CVU 953741).

Institutional Review Board Statement: The study was approved by the Institutional Review Board and the Ethics Committee of the Mexican Institute of Social Security (National Committee of Scientific Research) protocol number: R-2021-1305-011, date 18 October 2021.

Informed Consent Statement: Not applicable.

Data Availability Statement: The RNAseq data presented in this study are openly available in the Gene Expression Omnibus (GEO) database repository (<https://www.ncbi.nlm.nih.gov/geo>, accessed on 12 December 2022), with the GEO accession number GSE221082.

Acknowledgments: The authors would like to thank the assistance of Karen Lilith Gonzalez-Martinez for GSEA visualization and interpretation, as well as Leonardo Fernandez-Avila for the statistical analysis. We also thank Didier Trono for donating the plasmids pCMVR8.74 and pMD2.G.

Conflicts of Interest: The authors declare no conflict of interest.

References

1. Buskwofie, A.; David-West, G.; Clare, C.A. A Review of Cervical Cancer: Incidence and Disparities. *J. Natl. Med. Assoc.* **2020**, *112*, 229–232. [[CrossRef](#)] [[PubMed](#)]
2. Arbyn, M.; Weiderpass, E.; Bruni, L.; de Sanjosé, S.; Saraiya, M.; Ferlay, J.; Bray, F. Estimates of incidence and mortality of cervical cancer in 2018: A worldwide analysis. *Lancet Glob. Health* **2020**, *8*, e191–e203. [[CrossRef](#)] [[PubMed](#)]
3. Bray, F.; Ferlay, J.; Soerjomataram, I.; Siegel, R.L.; Torre, L.A.; Jemal, A. Global cancer statistics 2018: GLOBOCAN estimates of incidence and mortality worldwide for 36 cancers in 185 countries. *CA Cancer J. Clin.* **2018**, *68*, 394–424. [[CrossRef](#)] [[PubMed](#)]
4. Prendiville, W.S.R. *Colposcopy and Treatment of Cervical Precancer*; World Health Organization: Geneva, Switzerland, 2017; Volume 45, p. 178.
5. Zhou, J.; Wu, S.G.; Sun, J.Y.; Li, F.Y.; Lin, H.X.; Chen, Q.H.; He, Z.Y. Comparison of clinical outcomes of squamous cell carcinoma, adenocarcinoma, and adenosquamous carcinoma of the uterine cervix after definitive radiotherapy: A population-based analysis. *J. Cancer Res. Clin. Oncol.* **2017**, *143*, 115–122. [[CrossRef](#)]
6. Lu, X.; Jiang, L.; Zhang, L.; Zhu, Y.; Hu, W.; Wang, J.; Ruan, X.; Xu, Z.; Meng, X.; Gao, J.; et al. Immune Signature-Based Subtypes of Cervical Squamous Cell Carcinoma Tightly Associated with Human Papillomavirus Type 16 Expression, Molecular Features, and Clinical Outcome. *Neoplasia* **2019**, *21*, 591–601. [[CrossRef](#)]
7. Manini, I.; Montomoli, E. Epidemiology and prevention of Human Papillomavirus. *Ann. Di Ig. Med. Prev. E Di Comunita* **2018**, *30*, 28–32. [[CrossRef](#)]
8. Chan, C.K.; Aimagambetova, G.; Ukybassova, T.; Kongrtay, K.; Azizan, A. Human Papillomavirus Infection and Cervical Cancer: Epidemiology, Screening, and Vaccination-Review of Current Perspectives. *J. Oncol.* **2019**, *2019*, 3257939. [[CrossRef](#)]

9. Kaliff, M.; Sorbe, B.; Bohr Mordhorst, L.; Helenius, G.; Karlsson, M.G.; Lillsunde-Larsson, G. Findings of multiple HPV genotypes in cervical carcinoma are associated with poor cancer-specific survival in a Swedish cohort of cervical cancer primarily treated with radiotherapy. *Oncotarget* **2018**, *9*, 18786. [[CrossRef](#)]
10. Vats, A.; Trejo-Cerro, O.; Thomas, M.; Banks, L. Human papillomavirus E6 and E7: What remains? *Tumour Virus Res.* **2021**, *11*, 200213. [[CrossRef](#)]
11. Gutiérrez-Hoya, A.; Soto-Cruz, I. Role of the JAK/STAT Pathway in Cervical Cancer: Its Relationship with HPV E6/E7 Oncoproteins. *Cells* **2020**, *9*, 2297. [[CrossRef](#)]
12. Cospér, P.F.; McNair, C.; González, I.; Wong, N.; Knudsen, K.E.; Chen, J.J.; Markovina, S.; Schwarz, J.K.; Grigsby, P.W.; Wang, X. Decreased local immune response and retained HPV gene expression during chemoradiotherapy are associated with treatment resistance and death from cervical cancer. *Int. J. Cancer* **2020**, *146*, 2047–2058. [[CrossRef](#)] [[PubMed](#)]
13. Yeo-Teh, N.S.L.; Ito, Y.; Jha, S. High-Risk Human Papillomaviral Oncogenes E6 and E7 Target Key Cellular Pathways to Achieve Oncogenesis. *Int. J. Mol. Sci.* **2018**, *19*, 1706. [[CrossRef](#)] [[PubMed](#)]
14. Mailer, R.K.W. Alternative Splicing of FOXP3-Virtue and Vice. *Front. Immunol.* **2018**, *9*, 530. [[CrossRef](#)] [[PubMed](#)]
15. Kaur, G.; Goodall, J.C.; Jarvis, L.B.; Hill Gaston, J.S. Characterisation of Foxp3 splice variants in human CD4+ and CD8+ T cells—identification of Foxp3 Δ 7 in human regulatory T cells. *Mol. Immunol.* **2010**, *48*, 321–332. [[CrossRef](#)]
16. Williams, L.M.; Rudensky, A.Y. Maintenance of the Foxp3-dependent developmental program in mature regulatory T cells requires continued expression of Foxp3. *Nat. Immunol.* **2007**, *8*, 277–284. [[CrossRef](#)] [[PubMed](#)]
17. Deng, G.; Song, X.; Fujimoto, S.; Piccirillo, C.A.; Nagai, Y.; Greene, M.I. Foxp3 Post-translational Modifications and Treg Suppressive Activity. *Front. Immunol.* **2019**, *10*, 2486. [[CrossRef](#)]
18. Fleskens, V.; Minutti, C.M.; Wu, X.; Wei, P.; Pals, C.E.G.M.; McCrae, J.; Hemmers, S.; Groenewold, V.; Vos, H.-J.; Rudensky, A.; et al. Nemo-like Kinase Drives Foxp3 Stability and Is Critical for Maintenance of Immune Tolerance by Regulatory T Cells. *Cell Rep.* **2019**, *26*, 3600–3612.e3606. [[CrossRef](#)]
19. Du, J.; Huang, C.; Zhou, B.; Ziegler, S.F. Isoform-specific inhibition of ROR alpha-mediated transcriptional activation by human FOXP3. *J. Immunol.* **2008**, *180*, 4785–4792. [[CrossRef](#)]
20. Ichiyama, K.; Yoshida, H.; Wakabayashi, Y.; Chinen, T.; Saeki, K.; Nakaya, M.; Takaesu, G.; Hori, S.; Yoshimura, A.; Kobayashi, T. Foxp3 inhibits ROR γ mat-mediated IL-17A mRNA transcription through direct interaction with ROR γ mat. *J. Biol. Chem.* **2008**, *283*, 17003–17008. [[CrossRef](#)]
21. Sambucci, M.; Gargano, F.; De Rosa, V.; De Bardi, M.; Picozza, M.; Placido, R.; Ruggieri, S.; Capone, A.; Gasperini, C.; Matarese, G.; et al. FoxP3 isoforms and PD-1 expression by T regulatory cells in multiple sclerosis. *Sci. Rep.* **2018**, *8*, 3674. [[CrossRef](#)]
22. Li, L.; Xu, X.T.; Wang, L.L.; Qin, S.B.; Zhou, J.Y. Expression and clinicopathological significance of Foxp3 and VISTA in cervical cancer. *Am. J. Transl. Res.* **2021**, *13*, 10428–10438. [[PubMed](#)]
23. Litwin, T.R.; Irvin, S.R.; Chornock, R.L.; Sahasrabudhe, V.V.; Stanley, M.; Wentzensen, N. Infiltrating T-cell markers in cervical carcinogenesis: A systematic review and meta-analysis. *Br. J. Cancer* **2021**, *124*, 831–841. [[CrossRef](#)] [[PubMed](#)]
24. Chen, G.Y.; Chen, C.; Wang, L.; Chang, X.; Zheng, P.; Liu, Y. Cutting edge: Broad expression of the FoxP3 locus in epithelial cells: A caution against early interpretation of fatal inflammatory diseases following in vivo depletion of FoxP3-expressing cells. *J. Immunol.* **2008**, *180*, 5163–5166. [[CrossRef](#)]
25. Alfaar, A.S.; Stürzbecher, L.; Diedrichs-Möhning, M.; Lam, M.; Roubeix, C.; Ritter, J.; Schumann, K.; Annamalai, B.; Pompös, I.-M.; Rohrer, B.; et al. FoxP3 expression by retinal pigment epithelial cells: Transcription factor with potential relevance for the pathology of age-related macular degeneration. *J. Neuroinflammation* **2022**, *19*, 260. [[CrossRef](#)]
26. Karanikou, V.; Speletas, M.; Zamanakou, M.; Kalala, F.; Loules, G.; Kerenidi, T.; Barda, A.K.; Gourgoulianis, K.I.; Germentis, A.E. Foxp3 expression in human cancer cells. *J. Transl. Med.* **2008**, *6*, 19. [[CrossRef](#)]
27. Jia, H.; Qi, H.; Gong, Z.; Yang, S.; Ren, J.; Liu, Y.; Li, M.-Y.; Chen, G.G. The expression of FOXP3 and its role in human cancers. *Biochim. Et Biophys. Acta (BBA) Rev. Cancer* **2019**, *1871*, 170–178. [[CrossRef](#)] [[PubMed](#)]
28. Zuo, T.; Liu, R.; Zhang, H.; Chang, X.; Liu, Y.; Wang, L.; Zheng, P.; Liu, Y. FOXP3 is a novel transcriptional repressor for the breast cancer oncogene SKP2. *J. Clin. Investig.* **2007**, *117*, 3765–3773. [[CrossRef](#)]
29. Zuo, T.; Wang, L.; Morrison, C.; Chang, X.; Zhang, H.; Li, W.; Liu, Y.; Wang, Y.; Liu, X.; Chan, M.W.Y.; et al. FOXP3 is an X-linked breast cancer suppressor gene and an important repressor of the HER-2/ErbB2 oncogene. *Cell* **2007**, *129*, 1275–1286. [[CrossRef](#)] [[PubMed](#)]
30. Douglass, S.; Ali, S.; Meeson, A.P.; Browell, D.; Kirby, J.A. The role of FOXP3 in the development and metastatic spread of breast cancer. *Cancer Metastasis Rev.* **2012**, *31*, 843–854. [[CrossRef](#)]
31. Wang, L.; Liu, R.; Li, W.; Chen, C.; Katoh, H.; Chen, G.-Y.; McNally, B.; Lin, L.; Zhou, P.; Zuo, T.; et al. Somatic single hits inactivate the X-linked tumor suppressor FOXP3 in the prostate. *Cancer Cell* **2009**, *16*, 336–346. [[CrossRef](#)]
32. Zhang, H.Y.; Sun, H. Up-regulation of Foxp3 inhibits cell proliferation, migration and invasion in epithelial ovarian cancer. *Cancer Lett.* **2010**, *287*, 91–97. [[CrossRef](#)] [[PubMed](#)]
33. Chu, R.; Liu, S.Y.W.; Vlantis, A.C.; van Hasselt, C.A.; Ng, E.K.W.; Fan, M.D.; Ng, S.K.; Chan, A.B.W.; Du, J.; Wei, W.; et al. Inhibition of Foxp3 in cancer cells induces apoptosis of thyroid cancer cells. *Mol. Cell. Endocrinol.* **2015**, *399*, 228–234. [[CrossRef](#)] [[PubMed](#)]

34. Hinz, S.; Pagerols-Raluy, L.; Oberg, H.H.; Ammerpohl, O.; Grussel, S.; Sipos, B.; Grutzmann, R.; Pilarsky, C.; Ungefroren, H.; Saeger, H.D.; et al. Foxp3 expression in pancreatic carcinoma cells as a novel mechanism of immune evasion in cancer. *Cancer Res.* **2007**, *67*, 8344–8350. [[CrossRef](#)] [[PubMed](#)]
35. Kim, M.; Grimmig, T.; Grimm, M.; Lazariotou, M.; Meier, E.; Rosenwald, A.; Tsauro, I.; Blaheta, R.; Heemann, U.; Germer, C.T.; et al. Expression of Foxp3 in colorectal cancer but not in Treg cells correlates with disease progression in patients with colorectal cancer. *PLoS ONE* **2013**, *8*, e53630. [[CrossRef](#)]
36. Jou, Y.C.; Tsai, Y.S.; Lin, C.T.; Tung, C.L.; Shen, C.H.; Tsai, H.T.; Yang, W.H.; Chang, H.I.; Chen, S.Y.; Tzai, T.S. Foxp3 enhances HIF-1 α target gene expression in human bladder cancer through decreasing its ubiquitin-proteasomal degradation. *Oncotarget* **2016**, *7*, 65403–65417. [[CrossRef](#)]
37. Zhang, L.; Xu, J.; Zhang, X.; Zhang, Y.; Wang, L.; Huang, X.; Xu, Z. The Role of Tumoral FOXP3 on Cell Proliferation, Migration, and Invasion in Gastric Cancer. *Cell. Physiol. Biochem.* **2017**, *42*, 1739–1754. [[CrossRef](#)] [[PubMed](#)]
38. Jia, H.; Qi, H.; Peng, J.; Li, M.; Chen, G.G. FOXP3 Δ 3, the major isoform of FOXP3, promotes proliferation, migration, and invasion in non-small cell lung cancer. *Ann. Oncol.* **2019**, *30*, ii5–ii6. [[CrossRef](#)]
39. Zeng, C.; Yao, Y.; Jie, W.; Zhang, M.; Hu, X.; Zhao, Y.; Wang, S.; Yin, J.; Song, Y. Up-regulation of Foxp3 participates in progression of cervical cancer. *Cancer Immunol. Immunother. CII* **2012**, *62*, 481–487. [[CrossRef](#)]
40. Luo, Q.; Zhang, S.; Wei, H.; Pang, X.; Zhang, H. Roles of Foxp3 in the occurrence and development of cervical cancer. *Int. J. Clin. Exp. Pathol.* **2015**, *8*, 8717–8730.
41. Ye, J.; Coulouris, G.; Zaretskaya, I.; Cutcutache, I.; Rozen, S.; Madden, T.L. Primer-BLAST: A tool to design target-specific primers for polymerase chain reaction. *BMC Bioinform.* **2012**, *13*, 134. [[CrossRef](#)]
42. Okonechnikov, K.; Golosova, O.; Fursov, M. Unipro UGENE: A unified bioinformatics toolkit. *Bioinformatics* **2012**, *28*, 1166–1167. [[CrossRef](#)] [[PubMed](#)]
43. Team, R. *RStudio: Integrated Development for R*; 1.4.1717; RStudio, Inc.: Boston, MA, USA, 2015.
44. Afgan, E.; Baker, D.; Batut, B.; van den Beek, M.; Bouvier, D.; Čech, M.; Chilton, J.; Clements, D.; Coraor, N.; Grüning, B.A.; et al. The Galaxy platform for accessible, reproducible and collaborative biomedical analyses: 2018 update. *Nucleic Acids Res.* **2018**, *46*, W537–W544. [[CrossRef](#)] [[PubMed](#)]
45. Andrews, S. FastQC A Quality Control tool for High Throughput Sequence Data. 2010. Available online: <http://www.bioinformatics.babraham.ac.uk/projects/fastqc> (accessed on 3 February 2022).
46. Liao, Y.; Smyth, G.K.; Shi, W. The R package Rsubread is easier, faster, cheaper and better for alignment and quantification of RNA sequencing reads. *Nucleic Acids Res.* **2019**, *47*, e47. [[CrossRef](#)] [[PubMed](#)]
47. Liao, Y.; Smyth, G.K.; Shi, W. featureCounts: An efficient general purpose program for assigning sequence reads to genomic features. *Bioinformatics* **2013**, *30*, 923–930. [[CrossRef](#)] [[PubMed](#)]
48. Love, M.I.; Huber, W.; Anders, S. Moderated estimation of fold change and dispersion for RNA-seq data with DESeq2. *Genome Biol.* **2014**, *15*, 550. [[CrossRef](#)] [[PubMed](#)]
49. Subramanian, A.; Tamayo, P.; Mootha, V.K.; Mukherjee, S.; Ebert, B.L.; Gillette, M.A.; Paulovich, A.; Pomeroy, S.L.; Golub, T.R.; Lander, E.S.; et al. Gene set enrichment analysis: A knowledge-based approach for interpreting genome-wide expression profiles. *Proc. Natl. Acad. Sci. USA* **2005**, *102*, 15545–15550. [[CrossRef](#)]
50. Tang, G.; Cho, M.; Wang, X. OncoDB: An interactive online database for analysis of gene expression and viral infection in cancer. *Nucleic Acids Res.* **2022**, *50*, D1334–D1339. [[CrossRef](#)]
51. Gao, J.; Aksoy, B.A.; Dogrusoz, U.; Dresdner, G.; Gross, B.; Sumer, S.O.; Sun, Y.; Jacobsen, A.; Sinha, R.; Larsson, E.; et al. Integrative analysis of complex cancer genomics and clinical profiles using the cBioPortal. *Sci. Signal* **2013**, *6*, p11. [[CrossRef](#)]
52. Cerami, E.; Gao, J.; Dogrusoz, U.; Gross, B.E.; Sumer, S.O.; Aksoy, B.A.; Jacobsen, A.; Byrne, C.J.; Heuer, M.L.; Larsson, E.; et al. The cBio Cancer Genomics Portal: An Open Platform for Exploring Multidimensional Cancer Genomics Data. *Cancer Discov.* **2012**, *2*, 401–404. [[CrossRef](#)]
53. Yang, I.S.; Son, H.; Kim, S.; Kim, S. ISOexpresso: A web-based platform for isoform-level expression analysis in human cancer. *BMC Genom.* **2016**, *17*, 631. [[CrossRef](#)]
54. Sun, W.; Duan, T.; Ye, P.; Chen, K.; Zhang, G.; Lai, M.; Zhang, H. TSVdb: A web-tool for TCGA splicing variants analysis. *BMC Genom.* **2018**, *19*, 405. [[CrossRef](#)] [[PubMed](#)]
55. Zheng, Y.; Josefowicz, S.Z.; Kas, A.; Chu, T.T.; Gavin, M.A.; Rudensky, A.Y. Genome-wide analysis of Foxp3 target genes in developing and mature regulatory T cells. *Nature* **2007**, *445*, 936–940. [[CrossRef](#)] [[PubMed](#)]
56. Wu, L.; Yi, B.; Wei, S.; Rao, D.; He, Y.; Naik, G.; Bae, S.; Liu, X.M.; Yang, W.H.; Sonpavde, G.; et al. Loss of FOXP3 and TSC1 Accelerates Prostate Cancer Progression through Synergistic Transcriptional and Posttranslational Regulation of c-MYC. *Cancer Res.* **2019**, *79*, 1413–1425. [[CrossRef](#)] [[PubMed](#)]
57. Zhang, H.; Prado, K.; Zhang, K.X.; Peek, E.M.; Lee, J.; Wang, X.; Huang, J.; Li, G.; Pellegrini, M.; Chin, A.I. Biased Expression of the FOXP3 Δ 3 Isoform in Aggressive Bladder Cancer Mediates Differentiation and Cisplatin Chemotherapy Resistance. *Clin Cancer Res.* **2016**, *22*, 5349–5361. [[CrossRef](#)]
58. Lopes, J.E.; Torgerson, T.R.; Schubert, L.A.; Anover, S.D.; Ocheltree, E.L.; Ochs, H.D.; Ziegler, S.F. Analysis of FOXP3 Reveals Multiple Domains Required for Its Function as a Transcriptional Repressor. *J. Immunol.* **2006**, *177*, 3133–3142. [[CrossRef](#)]
59. Chae, W.J.; Henegariu, O.; Lee, S.K.; Bothwell, A.L. The mutant leucine-zipper domain impairs both dimerization and suppressive function of Foxp3 in T cells. *Proc. Natl. Acad. Sci. USA* **2006**, *103*, 9631–9636. [[CrossRef](#)]

60. van der Vliet, H.J.; Nieuwenhuis, E.E. IPEX as a result of mutations in FOXP3. *Clin. Dev. Immunol.* **2007**, *2007*, 89017. [[CrossRef](#)]
61. Magg, T.; Wiebking, V.; Conca, R.; Krebs, S.; Arens, S.; Schmid, I.; Klein, C.; Albert, M.H.; Hauck, F. IPEX due to an exon 7 skipping FOXP3 mutation with autoimmune diabetes mellitus cured by selective TReg cell engraftment. *Clin. Immunol.* **2018**, *191*, 52–58. [[CrossRef](#)]
62. Mailer, R.K.; Falk, K.; Rotzschke, O. Absence of leucine zipper in the natural FOXP3Delta2Delta7 isoform does not affect dimerization but abrogates suppressive capacity. *PLoS ONE* **2009**, *4*, e6104. [[CrossRef](#)]
63. Lv, J.H.; Wang, F.; Shen, M.H.; Wang, X.; Zhou, X.J. SATB1 expression is correlated with β -catenin associated epithelial-mesenchymal transition in colorectal cancer. *Cancer Biol. Ther.* **2016**, *17*, 254–261. [[CrossRef](#)]
64. Mao, L.J.; Yang, C.H.; Fan, L.; Gao, P.; Yang, D.R.; Xue, B.X.; Zheng, J.N.; Shan, Y.X. SATB1 promotes prostate cancer metastasis by the regulation of epithelial-mesenchymal transition. *Biomed Pharm.* **2016**, *79*, 1–8. [[CrossRef](#)] [[PubMed](#)]
65. Glatzel-Plucinska, N.; Piotrowska, A.; Rzechonek, A.; Podhorska-Okolow, M.; Dziegiel, P. SATB1 protein is associated with the epithelial-mesenchymal transition process in non-small cell lung cancers. *Oncol. Rep.* **2021**, *45*, 118. [[CrossRef](#)] [[PubMed](#)]
66. Huo, F.-C.; Pan, Y.-J.; Li, T.-T.; Mou, J.; Pei, D.-S. PAK5 promotes the migration and invasion of cervical cancer cells by phosphorylating SATB1. *Cell Death Differ.* **2019**, *26*, 994–1006. [[CrossRef](#)] [[PubMed](#)]
67. Wang, S.; Zeng, J.; Xiao, R.; Xu, G.; Liu, G.; Xiong, D.; Ye, Y.; Chen, B.; Wang, H.; Luo, Q.; et al. Poor prognosis and SATB1 overexpression in solid tumors: A meta-analysis. *Cancer Manag. Res.* **2018**, *10*, 1471–1478. [[CrossRef](#)]
68. Zhao, L.; Zheng, Y.; Ji, Y.; Zhang, X. The expression of special AT-rich binding protein 1 in cervical cancer and its clinical significance. *Oncol. Targets Ther.* **2019**, *12*, 945–951. [[CrossRef](#)]
69. Pan, Y.; Bai, C.B.; Joyner, A.L.; Wang, B. Sonic hedgehog signaling regulates Gli2 transcriptional activity by suppressing its processing and degradation. *Mol. Cell Biol.* **2006**, *26*, 3365–3377. [[CrossRef](#)]
70. Ichimiya, S.; Onishi, H.; Nagao, S.; Koga, S.; Sakihama, K.; Nakayama, K.; Fujimura, A.; Oyama, Y.; Imaizumi, A.; Oda, Y.; et al. GLI2 but not GLI1/GLI3 plays a central role in the induction of malignant phenotype of gallbladder cancer. *Oncol Rep.* **2021**, *45*, 997–1010. [[CrossRef](#)]
71. Lu, Y.; Zhang, B.; Wang, B.; Wu, D.; Wang, C.; Gao, Y.; Liang, W.; Xi, H.; Wang, X.; Chen, L. MiR-144-3p inhibits gastric cancer progression and stemness via directly targeting GLI2 involved in hedgehog pathway. *J. Transl. Med.* **2021**, *19*, 432. [[CrossRef](#)]
72. Zhu, H.; Xia, L.; Shen, Q.; Zhao, M.; Gu, X.; Bouamar, H.; Wang, B.; Sun, L.Z.; Zhu, X. Differential effects of GLI2 and GLI3 in regulating cervical cancer malignancy in vitro and in vivo. *Lab. Investig.* **2018**, *98*, 1384–1396. [[CrossRef](#)]
73. Riihilä, P.; Viiklepp, K.; Nissinen, L.; Farshchian, M.; Kallajoki, M.; Kivisaari, A.; Meri, S.; Peltonen, J.; Peltonen, S.; Kähäri, V.M. Tumour-cell-derived complement components C1r and C1s promote growth of cutaneous squamous cell carcinoma. *Br. J. Dermatol.* **2020**, *182*, 658–670. [[CrossRef](#)]
74. Viiklepp, K.; Nissinen, L.; Ojalil, M.; Riihilä, P.; Kallajoki, M.; Meri, S.; Heino, J.; Kähäri, V.M. C1r Upregulates Production of Matrix Metalloproteinase-13 and Promotes Invasion of Cutaneous Squamous Cell Carcinoma. *J. Invest. Dermatol.* **2022**, *142*, 1478–1488. [[CrossRef](#)] [[PubMed](#)]
75. Gürz, S.; Çelik, B.; Menteşe, A.; Us Altay, D. Diagnostic value of signal peptide-Complement C1r/C1s, Uegf, and Bmp1-epidermal growth factor domain-containing protein 1 on serum and tissue samples in non-small cell lung cancer. *Turk. Gogus Kalp. Damar. Cerrahisi Derg.* **2018**, *26*, 246–253. [[CrossRef](#)] [[PubMed](#)]
76. Kanao, H.; Enomoto, T.; Kimura, T.; Fujita, M.; Nakashima, R.; Ueda, Y.; Ueno, Y.; Miyatake, T.; Yoshizaki, T.; Buzard, G.S.; et al. Overexpression of LAMP3/TSC403/DC-LAMP promotes metastasis in uterine cervical cancer. *Cancer Res.* **2005**, *65*, 8640–8645. [[CrossRef](#)] [[PubMed](#)]
77. Bettelli, E.; Dastrange, M.; Oukka, M. Foxp3 interacts with nuclear factor of activated T cells and NF-kappa B to repress cytokine gene expression and effector functions of T helper cells. *Proc. Natl. Acad. Sci. USA* **2005**, *102*, 5138–5143. [[CrossRef](#)]
78. Niu, J.; Jiang, C.; Li, C.; Liu, L.; Li, K.; Jian, Z.; Gao, T. Foxp3 expression in melanoma cells as a possible mechanism of resistance to immune destruction. *Cancer Immunol. Immunother.* **2011**, *60*, 1109–1118. [[CrossRef](#)]
79. Downward, J. Role of receptor tyrosine kinases in G-protein-coupled receptor regulation of Ras: Transactivation or parallel pathways? *Biochem. J.* **2003**, *376*, e9–e10. [[CrossRef](#)]
80. Perera, D.; Venkitaraman, A.R. Oncogenic KRAS triggers MAPK-dependent errors in mitosis and MYC-dependent sensitivity to anti-mitotic agents. *Sci. Rep.* **2016**, *6*, 29741. [[CrossRef](#)]
81. Hamarsheh, S.a.; Groß, O.; Brummer, T.; Zeiser, R. Immune modulatory effects of oncogenic KRAS in cancer. *Nat. Commun.* **2020**, *11*, 5439. [[CrossRef](#)]
82. Zhang, Y.; Zhao, W.; Na, F.; Li, M.; Tong, S. LINC01354/microRNA-216b/KRAS Axis Promotes the Occurrence and Metastasis of Endometrial Cancer. *Nanoscale Res. Lett.* **2022**, *17*, 21. [[CrossRef](#)]
83. Liao, W.; Overman, M.J.; Boutin, A.T.; Shang, X.; Zhao, D.; Dey, P.; Li, J.; Wang, G.; Lan, Z.; Li, J.; et al. KRAS-IRF2 Axis Drives Immune Suppression and Immune Therapy Resistance in Colorectal Cancer. *Cancer Cell* **2019**, *35*, 559–572. [[CrossRef](#)]
84. Tsujino, T.; Sugito, N.; Taniguchi, K.; Honda, R.; Komura, K.; Yoshikawa, Y.; Takai, T.; Minami, K.; Kuranaga, Y.; Shinohara, H.; et al. MicroRNA-143/Musashi-2/KRAS cascade contributes positively to carcinogenesis in human bladder cancer. *Cancer Sci.* **2019**, *110*, 2189–2199. [[CrossRef](#)] [[PubMed](#)]
85. Tang, A.H.; Hofer, R.A.; Guye, M.L.; Bear, H.D. Persistent EGFR/K-RAS/SIAH pathway activation drives chemo-resistance and early tumor relapse in triple-negative breast cancer. *Cancer Drug Resist.* **2022**, *5*, 691–702. [[CrossRef](#)] [[PubMed](#)]

86. Wegman, P.; Ahlin, C.; Sorbe, B. Genetic Alterations in the K-Ras Gene Influence the Prognosis in Patients With Cervical Cancer Treated by Radiotherapy. *Int. J. Gynecol. Cancer* **2011**, *21*, 86. [[CrossRef](#)]
87. Ramos-Solano, M.; Meza-Canales, I.D.; Torres-Reyes, L.A.; Alvarez-Zavala, M.; Alvarado-Ruiz, L.; Rincon-Orozco, B.; Garcia-Chagollan, M.; Ochoa-Hernández, A.B.; Ortiz-Lazareno, P.C.; Rösl, F.; et al. Expression of WNT genes in cervical cancer-derived cells: Implication of WNT7A in cell proliferation and migration. *Exp. Cell Res.* **2015**, *335*, 39–50. [[CrossRef](#)]
88. Mir, R.; Pradhan, S.J.; Patil, P.; Mulherkar, R.; Galande, S. Wnt/ β -catenin signaling regulated SATB1 promotes colorectal cancer tumorigenesis and progression. *Oncogene* **2016**, *35*, 1679–1691. [[CrossRef](#)]
89. Ruan, K.; Song, G.; Ouyang, G. Role of hypoxia in the hallmarks of human cancer. *J. Cell Biochem.* **2009**, *107*, 1053–1062. [[CrossRef](#)] [[PubMed](#)]
90. Jing, X.; Yang, F.; Shao, C.; Wei, K.; Xie, M.; Shen, H.; Shu, Y. Role of hypoxia in cancer therapy by regulating the tumor microenvironment. *Mol. Cancer* **2019**, *18*, 157. [[CrossRef](#)]
91. Emami Nejad, A.; Najafgholian, S.; Rostami, A.; Sistani, A.; Shojaeifar, S.; Esparvarinha, M.; Nedaenia, R.; Haghjooy Javanmard, S.; Taherian, M.; Ahmadi, M.; et al. The role of hypoxia in the tumor microenvironment and development of cancer stem cell: A novel approach to developing treatment. *Cancer Cell Int.* **2021**, *21*, 62. [[CrossRef](#)]
92. Yan, B.; Ma, Q.F.; Tan, W.F.; Cai, H.N.; Li, Y.L.; Zhou, Z.G.; Dai, X.; Zhu, F.X.; Xiong, Y.J.; Xu, M.; et al. Expression of HIF-1 α is a predictive marker of the efficacy of neoadjuvant chemotherapy for locally advanced cervical cancer. *Oncol. Lett.* **2020**, *20*, 841–849. [[CrossRef](#)]
93. Datta, A.; West, C.; O'Connor, J.P.B.; Choudhury, A.; Hoskin, P. Impact of hypoxia on cervical cancer outcomes. *Int. J. Gynecol. Cancer* **2021**, *31*, 1459–1470. [[CrossRef](#)]
94. Dehdashti, F.; Grigsby, P.W.; Lewis, J.S.; Laforest, R.; Siegel, B.A.; Welch, M.J. Assessing tumor hypoxia in cervical cancer by PET with ^{60}Cu -labeled diacetyl-bis(N4-methylthiosemicarbazone). *J. Nucl. Med.* **2008**, *49*, 201–205. [[CrossRef](#)] [[PubMed](#)]
95. Mujic, H.; Nagelkerke, A.; Rouschop, K.M.; Chung, S.; Chaudary, N.; Span, P.N.; Clarke, B.; Milosevic, M.; Sykes, J.; Hill, R.P.; et al. Hypoxic activation of the PERK/eIF2 α arm of the unfolded protein response promotes metastasis through induction of LAMP3. *Clin. Cancer Res.* **2013**, *19*, 6126–6137. [[CrossRef](#)] [[PubMed](#)]

Disclaimer/Publisher's Note: The statements, opinions and data contained in all publications are solely those of the individual author(s) and contributor(s) and not of MDPI and/or the editor(s). MDPI and/or the editor(s) disclaim responsibility for any injury to people or property resulting from any ideas, methods, instructions or products referred to in the content.